Seeding and Emergence of Composite Skyrmions in a van der Waals Magnet

Lukas Powalla,* Max T. Birch,* Kai Litzius, Sebastian Wintz, Fehmi S. Yasin, Luke A. Turnbull, Frank Schulz, Daniel A. Mayoh, Geetha Balakrishnan, Markus Weigand, Xiuzhen Yu, Klaus Kern, Gisela Schütz, and Marko Burghard

Topological charge plays a significant role in a range of physical systems. In particular, observations of real-space topological objects in magnetic materials have been largely limited to skyrmions – states with a unitary topological charge. Recently, more exotic states with varying topology, such as antiskyrmions, merons, or bimerons and 3D states such as skyrmion strings, chiral bobbers, and hopfions, have been experimentally reported. Along these lines, the realization of states with higher-order topology has the potential to open new avenues of research in topological magnetism and its spintronic applications. Here, real-space imaging of such spin textures, including skyrmion, skyrmionium, skyrmion bag, and skyrmion sack states, observed in exfoliated flakes of the van der Waals magnet $Fe_{3-x}GeTe_2$ (FGT) is reported. These composite skyrmions may emerge from seeded, loop-like states condensed into the stripe domain structure, demonstrating the possibility to realize spin textures with arbitrary integer topological charge within exfoliated flakes of 2D magnets. The general nature of the formation mechanism motivates the search for composite skyrmion states in both well-known and new magnetic materials, which may yet reveal an even richer spectrum of higher-order topological objects.

1. Introduction

In his original works, Tony Skyrme sought to provide an alternative theory of atomic nuclei, envisaging nucleons as solitonic excitations in a pion field,[1] forming topologically invariant knot-like particles which would later become known as skyrmions. Nuclei with greater atomic number can be modeled as composite states of multiple skyrmions, which exhibit increasingly higher integer topological charge.[2,3] From homotopy theory, this topological charge, or degree, Q can be defined as the number of wrappings of a vector field $\mathbf{n}$ over a unit a sphere – expressed mathematically,[4]

$$Q = \frac{1}{4\pi} \iint_s \mathbf{n} \cdot \left(\frac{\partial \mathbf{n}}{\partial x} \times \frac{\partial \mathbf{n}}{\partial y} \right) d^2\mathbf{r} \qquad (1)$$

States with the same Q can be smoothly deformed into one another, while discontinuous operations are required to transform between states with different topological charge.

Topology has subsequently been discovered to play a key role in a range of physical systems,[5–10] and real-space skyrmion-like topological objects have been observed in Bose-Einstein condensates,[11] liquid crystals,[7] bulk chiral magnets,[5,6] and magnetic thin films.[12,13] In magnetic systems, monochiral skyrmion states are typically stabilized by the presence of the Dzyaloshinskii-Moriya interaction (DMI) induced

L. Powalla, K. Kern, M. Burghard
Max Planck Institute for Solid State Research
70569, Stuttgart, Germany
E-mail: l.powalla@fkf.mpg.de

M. T. Birch, K. Litzius, S. Wintz, F. Schulz, G. Schütz
Max Planck Institute for Intelligent Systems
70569, Stuttgart, Germany
E-mail: birch@is.mpg.de

M. T. Birch, F. S. Yasin, X. Yu
RIKEN Center for Emergent Matter Science (CEMS)
Wako 351-0198, Japan

L. A. Turnbull
Department of Physics
Durham University
Durham DH1 3LE, UK

D. A. Mayoh, G. Balakrishnan
Department of Physics
University of Warwick
Coventry CV4 7AL, UK

M. Weigand
Institute Nanospectroscopy
Helmholtz-Zentrum Berlin
12489, Berlin, Germany

K. Kern
Institut de Physique
École Polytechnique Fédérale de Lausanne
Lausanne 1015, Switzerland

by the breaking of inversion symmetry.[4,14] These magnetic skyrmions have received significant attention over the past 10 years due to their possible application in racetrack and neuromorphic spintronic devices.[15] The majority of studies of magnetic systems have investigated 2D skyrmions with a unitary topological charge, $|Q| = 1$, or related states with $|Q| \leqslant 1$,[16–18] such as merons[19] or antiskyrmions.[20–22] In contrast, in liquid crystal systems, states with $|Q| > 1$ have often been observed in the form of hopfion, toron and skyrmion bag states.[8,23,24] It is only recently that more complex magnetic states have begun to be discovered, such as skyrmionium,[25–27] hopfion,[28] skyrmion bundle[29] and skyrmion braid[30] states. Theoretical and computational studies have predicted that chiral magnetic systems should be capable of hosting an essentially infinite number of 2D composite skyrmion states, with arbitrary integer topological degree.[24,31,32] However, a material capable of exhibiting multiple objects with a diverse range of topological states, and a method to induce their formation, has yet to be discovered.

The recent realization of few to monolayer exfoliated flakes of 2D van der Waals (vdW) magnets has opened up a new class of materials capable of hosting topological spin textures.[33,34] Skyrmions with $|Q| = 1$ have since been reported in thin flakes of $Cr_2Ge_2Te_6$,[35,36] and the target of the present study, Fe_3GeTe_2 (FGT).[37–44] Currently, it is suggested that these skyrmions are stabilized by a combination of the dipolar interaction and DMI. Owing to their atomically well-defined surfaces, these 2D magnets can be smoothly stacked together,[45,46] in contrast to typical sputtered multilayers, which often suffer from interlayer mixing and pronounced roughness. The stacking of 2D materials into vdW heterostructures enables the exploitation of interlayer proximity effects to fine-tune the properties of the magnetic layer,[47–49] allowing tailored magnetic states to be created. Hence, the discovery of higher-order topological spin textures in these materials would hold great promise for utilizing complex spin textures in future spintronic devices. Indeed, some prototype FGT devices have already been realized, including spin valve and spin-orbit torque devices.[50–53]

In this work, we report the observation of topological spin textures beyond skyrmions, hosted in exfoliated flakes of the 2D magnet FGT.[54,55] The associated magnetic phase diagram reveals a wide range of applied magnetic field and temperature where varied topological configurations of composite skyrmions can coexist. Accompanying micromagnetic simulations reproduce the seeding and emergence formation mechanism realized by random thermal fluctuations close to the Curie temperature, T_C. Our study of the transformations between objects with different topological charge raises questions about the role that topology plays in their stability.

2. Results

2.1. Composite Skyrmion Observation

We utilized scanning transmission X-ray microscopy (STXM) to investigate the spin textures within two exfoliated $Fe_{3-x}GeTe_2$ flakes, with $x = 0.03$ and 0.27, thickness of 90 and 80 nm, and T_C of 213 and 185 K, respectively.[56] The Fe deficiency is known to lower the T_C and uniaxial anisotropy in the material, driven by vacancies on the Fe (II) lattice site.[57,58] To facilitate the transmission measurements, the FGT flakes were transferred to X-ray transparent Si_3N_4 membranes and capped with hexaboron nitride (hBN) to prevent further oxidation (see Experimental Section, Figure S1, Supporting Information). Micrographs of a selection of magnetic objects observed in the FGT flakes are shown in **Figure 1**a–d, alongside vector visualizations. To categorize these spin textures, we turn to recent theoretical frameworks,[31,32] whereby the observed objects can be understood as
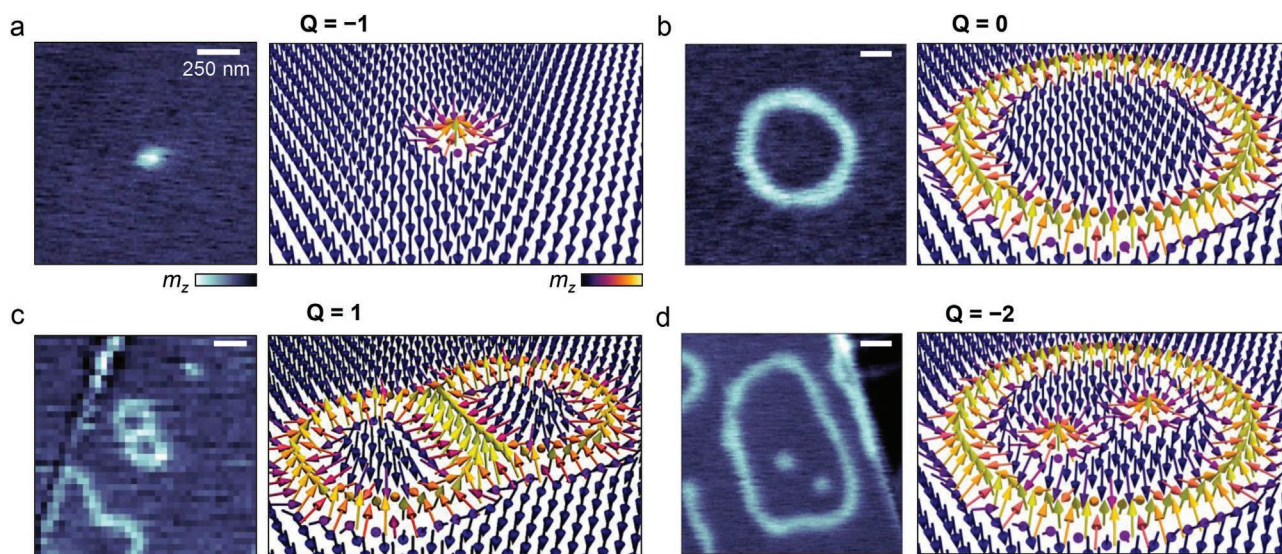

Figure 1. Real-space observations and visualizations of composite skyrmion states in the 2D magnet $Fe_{3-x}GeTe_2$ (FGT). a–d) Scanning transmission X-ray micrographs and schematic visualizations of composite skyrmion objects observed in the exfoliated FGT flakes, including skyrmion (a), skyrmionium (b), skyrmion bag (c), and skyrmion sack (d) states. In each case, the total topological charge Q is labeled. Images a-c are of the $x = 0.27$ flake, image d is of the $x = 0.03$ flake. The color map is proportional to the out-of-plane magnetization component, m_z. The schematic illustrations are mathematical constructions of the expected vector field demonstrating each spin configuration (details in Supporting Information).

composite states of skyrmions and skyrmioniums. The overall topological degree can be determined globally from Equation 1, or by considering the number and orientation of the closed magnetic domain walls which comprise each object.

An image of a single isolated skyrmion is shown in Figure 1a, with $Q = -1$ and diameter ≈100 nm. Previous observations have demonstrated FGT flakes with comparable thickness to ours possess Néel-type domain walls,[40–43] as indicated by the vector visualization. To check the type of domain wall of the present samples, we performed Lorentz transmission electron microscopy (LTEM) on a similar flake of the $x = 0.27$ composition (see Experimental Section). The results of the tilting experiment, where the magnetic domain contrast greatly increased at higher tilt angles, demonstrated the present spin textures also appear to exhibit Néel-type domain walls (Full LTEM data shown in Figures S2 and S3, Supporting Information). Further analysis of the domain wall profiles reveals a characteristic domain wall width of ≈90 nm. (see Figure S4, Supporting Information.)

Figure 1b exhibits an example of a skyrmionium state[26,59] (corresponding LTEM images of skyrmionium states in Figure S3, Supporting Information). These states have previously proved challenging to isolate, and have often been observed in confined geometries where they have been termed target skyrmions.[60–62] A skyrmionium can be considered as a $Q = 1$ skyrmion with a core parallel to the background magnetization, embedded within a larger skyrmion of the opposite magnetization and $Q = -1$, and thus the total state exhibits a global $Q = 0$. As a consequence of this, a skyrmionium does not exhibit deflection due to the skyrmion Hall effect under current-driven motion,[27] and they are therefore seen as an alternative to skyrmions as the storage element in racetrack memory device concepts.

Figure 1c-d reveals more complex, topologically non-trivial composite skyrmion states. The object presented in Figure 1c has previously been termed diskyrmionium,[25] as it is composed of two skyrmionium states with a shared domain wall. The state can be considered as two skyrmions of degree $Q = 1$ embedded within a single skyrmion with $Q = -1$, and thus with global $Q = 1$. This diskyrmionium is topologically equivalent to a skyrmion bag with two central skyrmions, reported previously in simulations.[24,31,63] Magnetic skyrmion bag states have so far only been experimentally observed within the bulk thickness of skyrmion bundles in FeGe lamellae[29] – in contrast, the state presented here should extend through the entire thickness of the FGT flake. Since the spin textures are primarily dipolar-stabilised we do not expect significant modulation of the magnetization along the out-of-plane direction for any of the observed states. Figure 1d depicts a $Q = -2$ composite state known as a skyrmion sack, composed of two skyrmions within an outer shell consisting of a skyrmionium, which has previously only been observed in simulations.[31,32,64]

2.2. Emergence from Seed States

The observed composite skyrmion states were realized by a specific magnetic field and temperature sample history: the FGT flakes were heated above T_C, and cooled under zero applied magnetic field (zero-field cooling, ZFC). This resulted in the formation of a complex domain structure, seeded with loop-like states within the magnetic stripes. For example, X-ray micrographs of the FGT flake measured at 135 K during a subsequent increase of the out-of-plane applied magnetic field are shown in **Figure 2**a–c, revealing the formation of skyrmionium states. In Figure 2d-f, we show a visualization of the magnetic domain walls within the FGT flake, allowing the emergence of the skyrmionium states to be visualized (see Experimental section, S5, Supporting Information). In each case, the regions shaded in magenta are those surrounded by two complete, closed-loop, magnetic domain walls. We have highlighted one such example by coloring two domain walls green and blue in Figure 2d,e. From our observations, these loop-like seed states are a necessary, but not sufficient, initial requirement to facilitate the formation of skyrmionium and higher-order composite skyrmion states (further micrographs shown in Figure S6, Supporting Information).

For comparison, we examined the possibility to realize composite skyrmion states following a field-sweep (protocol, where the flake was initialized in the saturated state at −250 mT and the magnetic field subsequently increased – a widely-utilized procedure for investigating spin texture formation. As shown in Figure 2g, by 20 mT the stripe domain state was nucleated, proliferating throughout the flake in a dendrite-like pattern. Due to the repulsion of neighboring domain walls from one another,[32] there is a large energy barrier preventing two of these stripes from connecting. This results in no loops within the domain structure, and therefore no potential for composite skyrmion formation, as demonstrated by the domain wall view in Figure 2h (further micrographs shown in Figure S7, Supporting Information). In contrast, for the ZFC measurements in Figure 2a–f, we suggest that the strong thermal fluctuations present as the sample is cooled through T_C enable the condensation of the loop-like seed states required for composite skyrmion formation. Thus, the specific traversal of the FGT flake's temperature and applied field history reveals these more complex topological states.

2.3. Composite Skyrmion Stability

We performed further imaging following the ZFC process at a range of temperatures to explore the stability of each spin texture (additional data shown in Figure S8, Supporting Information). The measurements are summarized by the magnetic phase diagram in **Figure 3**, which shows the field and temperature ranges where skyrmions and skyrmioniums emerged from the seeded stripe domain state, and annihilated into the uniformly magnetized state. In a few cases, skyrmionium and skyrmion states were formed directly upon ZFC, which are not shown here for clarity. Due to the comparatively lower chance for the formation of the skyrmion bag and sack states from the random ZFC seeding process, we do not have a sufficient sample size to determine their relative stability. However, the skyrmion bags with $Q \geqslant 1$ were observed within the same region as the basic skyrmionium states, while the skyrmion sacks with $Q \leqslant -1$ can be expected to be stable within the range where skyrmion and skyrmionium emergence overlaps. Therefore, we argue that all manner of composite skyrmion states
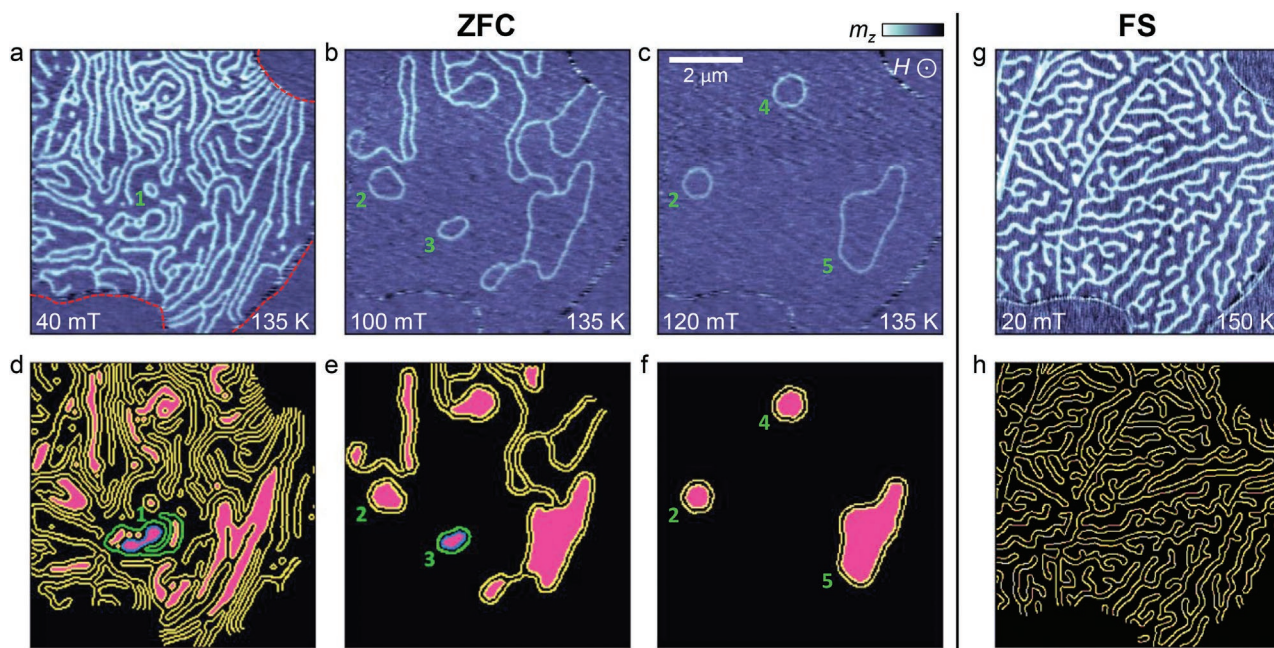
**ADVANCED
SCIENCE NEWS**

www.advancedsciencenews.com

**ADVANCED
MATERIALS**

www.advmat.de

Figure 2. Seeding and emergence of isolated skyrmionium states from loop-like stripe domains. a–c) Scanning transmission X-ray micrographs of the $Fe_{3-x}GeTe_2$ $x = 0.27$ flake as a function of increasing applied magnetic field at 135 K, revealing the formation of skyrmionium states, labeled 1–5. The sample was initialized by zero-field cooling (ZFC) from above T_C. The color map is proportional to the out-of-plane magnetization component, m_z. d–f) Visualizations of the magnetic domain walls as determined by an edge detection algorithm. Regions representing loop-like states with the correct configuration to become isolated skyrmionium, or higher-order, states are highlighted by the magenta fill. One example skyrmionium emergence is shown by the highlighted green and blue domain walls in d and e. g,h) X-ray micrograph and domain wall view of the FGT flake following a field sweep (FS) procedure at 150 K, where the magnetic field was increased starting from a uniformly magnetized state at −250 mT. The lack of magenta-filled regions in the nucleated stripe domain state demonstrates a lack of potential composite skyrmion. The red dashed lines in a) indicate the edge of the flake sample.

with arbitrary integer topological charge are simultaneously realizable within this overlap region.

At high temperatures, the thermal fluctuations are strong enough that all stripe and therefore skyrmionium states are broken up into skyrmions at small applied fields. However, sig-
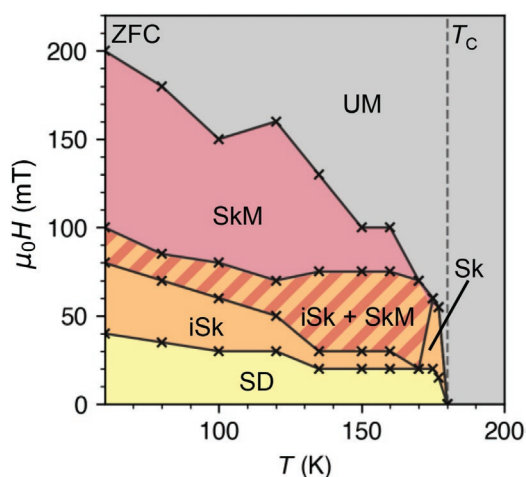
nificantly, for temperatures below 170 K, we observe that skyrmionium states can survive to higher applied magnetic fields than the skyrmions. With increasing field, the Zeeman energy is minimized by expanding domains with parallel magnetization, which results in a shrinking of the skyrmions to a minimum size before they are annihilated. Similarly, we observe that the area of the observed skyrmionium states decreases at higher applied fields. However, the field at which each skyrmionium is annihilated depends on its overall size: larger skyrmioniums survive to higher applied fields (Figure S9, Supporting Information). We suggest this increased stability is due to some combination of the lower domain wall curvature, and greater magnetic volume, which is not afforded to the comparably small magnetic skyrmions. We also observed that when reducing the field applied to a skyrmionium state, stripe domains were renucleated from the domain ring at lower applied fields. However, the loop-like seed state remained embedded within the stripe state, and reemerged upon increasing the field once again (Figure S10, Supporting Information). The realization of isolated composite skyrmion states in a uniform background at zero applied field remains a challenge.

Figure 3. Composite skyrmion formation phase diagram. Magnetic phase diagram of the $Fe_{3-x}GeTe_2$ $x = 0.27$ flake determined for increasing applied magnetic field after zero-field cooling (ZFC) from above T_C to each temperature. The formation of stripe domain (SD, yellow), skyrmion (Sk, orange), isolated skyrmions (iSk, orange), skyrmionium (SkM, red), and uniformly magnetized (UM, grey) states are indicated.

2.4. Topological Transitions

In **Figure 4**a–d, we exhibit observed transformations between a variety of the observed composite skyrmion states, together with the corresponding change in topological charge, ΔQ. The

2208930 (4 of 9)

**ADVANCED
SCIENCE NEWS**

www.advancedsciencenews.com
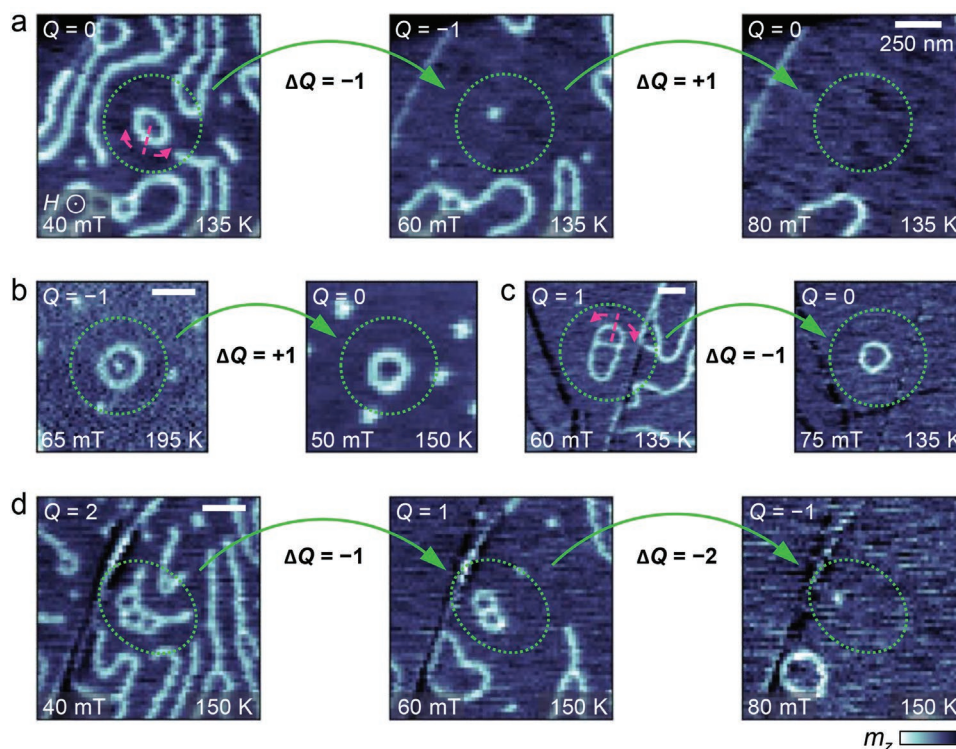
**ADVANCED
MATERIALS**

www.advmat.de

Figure 4. Topological transitions between composite skyrmion states. a–d) Sequential X-ray micrographs exhibiting the transformation of a skyrmionium into a skyrmion and finally into the uniform background; a) a skyrmion sack into a skyrmionium; b) a diskyrmionium into a skyrmionium; c) a triskyrmionium into a diskyrmionium into a skyrmion d). In each case, the total topological charge Q of each state, and its change between states ΔQ, are labeled. A suggestion of the observed collapse method is indicated by the magenta arrows in (a,c). The color map is proportional to the out-of-plane magnetization component, m_z.

annihilation of a skyrmionium into a skyrmion and finally into the uniformly magnetized background with increasing applied magnetic field is shown in Figure 4a. Similarly, Figure 4b–d reveals examples of the annihilation paths of skyrmion sack, diskyrmionium and triskyrmionium states, respectively. Each transition is realized by a cutting of a double domain wall, and the subsequent collapse of one lobe of the magnetization structure, as indicated by the magenta arrows in panels a and c, resulting in a change in the overall topological charge Q (see, e.g., sketches of collapse in Figure S10, Supporting Information).

This behavior has interesting implications for the role of topological protection of the observed states. In particular, in the case of skyrmionium, since it possesses the same topologically trivial $Q = 0$ as the uniform background state, from a mathematical perspective, it should be readily destroyed by a smooth deformation process (this is realized by a rotation of all the spins within the ring in the same direction around the central axis of the skyrmionium). Instead, the present observations indicate that the process of skyrmionium annihilation via a skyrmion state must possess a comparable, or lower, energy barrier than the smooth annihilation process afforded by its $Q = 0$ state, despite this requiring two changes in the topological charge. This strongly suggests that the preferred annihilation mechanisms, and therefore the stability, of the observed composite skyrmion states are not dominated by the mathematical concept of topological protection, which in reality is only as sig-

nificant as the physical energy barrier it represents. Instead, it is the energy landscape of the closed domain wall loops which give rise to the observed robustness of the skyrmionium and skyrmion bag states. We note that this does not mean that topology plays no role in the properties of these objects, which may still manifest in their emergent electrodynamics, such as the skyrmion and topological Hall effects.

The role of pinning in the stabilization of the observed composite skyrmion states should not be ignored – pinning sites may be responsible for the survival of the largest skyrmioniums at high applied magnetic fields, and also likely results in the additional tails of magnetization attached to some observed composite skyrmion states, such as the triskyrmionium exhibited in Figure 4d, and the extended size and irregular shape of some observed states. Nevertheless, to explore the possibility of reproducing the experimental behavior without pinning, we performed complementary micromagnetic simulations, modeling a ZFC cooling process by implementing thermal fluctuations (see Experimental Section). The simulated annealing procedure at 0 mT is shown in **Figure 5**a–d, revealing the seeding of familiar loop-like states within the stripe domains as the temperature is decreased. After the application of a range of applied magnetic fields, Figure 5e–h reveals the formation of numerous isolated composite skyrmion states, including skyrmions, skyrmioniums, and higher-order skyrmion bags,[24] well-reproducing the experimental results.
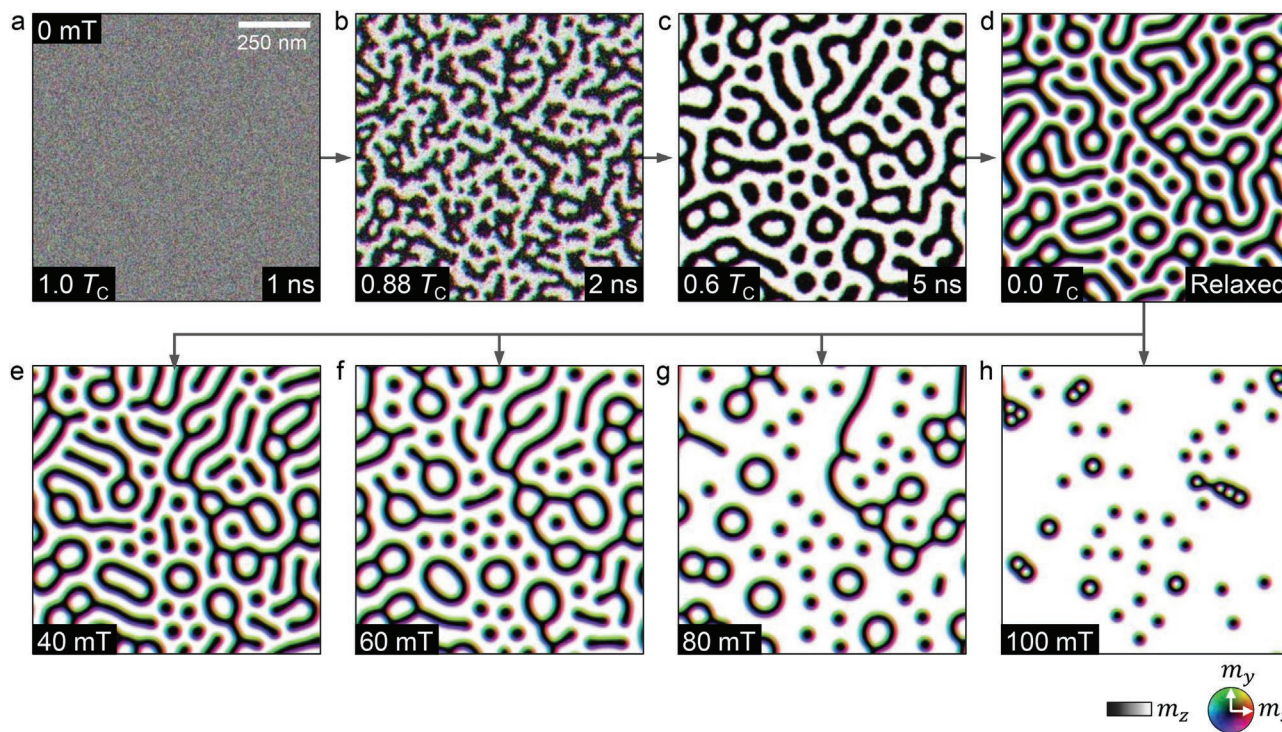
**ADVANCED
SCIENCE NEWS**

www.advancedsciencenews.com

**ADVANCED
MATERIALS**

www.advmat.de

Figure 5. Micromagnetic simulations of the composite skyrmion formation. a–f) Images of the simulated system during the annealing procedure. The randomized initial state is shown in (a), while (b) shows the first simulated step at a temperature below T_C, revealing the first formation of stripe domain states. As the thermal fluctuations are gradually reduced in (c,d), loop-like states emerge and stabilise within the stripe domain structure. e–h) Images of the simulated system after relaxation at a range of applied out-of-plane fields, demonstrating the formation of skyrmion, skyrmionium, diskyrmionium, and higher-order skyrmion bag states at 80 and 100 mT. The color map indicates both the out-of-plane magnetization component m_z, and the in-plane components m_x and m_y.

3. Conclusion

We have demonstrated that a wide range of isolated composite skyrmion states can be realized within a single system, created via the condensation of loop-like protostates within the magnetic stripe domains close to T_C, which are otherwise thermodynamically inaccessible to commonly explored experimental protocols. The discovery of these states in FGT flakes is particularly favorable, since they can be readily stacked with other 2D materials into heterostructures where the relevant magnetic parameters, such as the balance of the anisotropy and dipolar interactions with the DMI, can be tuned via proximity effects. Thus, the search for composite skyrmions in other newly discovered 2D magnets may prove fruitful, and could lead to the observation of even higher-order states, such as those with additional chiral kinks,[32] further widening the array of possible topological arrangements.

It remains to be seen whether the particular properties of FGT are responsible for the stability of the composite skyrmion states. Further studies should investigate the ideal material properties, such as sample thickness and the uniaxial anisotropy strength, for composite skyrmion formation. Due to their high T_C (typically above 400 K) and the community's focus on practical device applications, most studies of thin-film skyrmion systems have focused on room temperature measurements, besides a few exceptions.[65] Considering the specific thermal history required for composite skyrmion formation in

this work, it is possible that their existence in well-known systems has been overlooked. The formation process presented in this work results in a random assortment of composite skyrmions, with arbitrary size, position and topological degree. Further experiments could address the purposeful creation and control of these objects, for example, by local Joule heating or nucleation by injected spin currents. Moreover, detailed studies of the skyrmionium collapse would shed further light on the role that topology plays in the stability of these objects. The development of methods to tailor the properties of such higher-order topological configurations may lead to novel concepts for future information storage or reservoir computing devices.

4. Experimental Section

Sample Preparation and Characterization: Single crystals of $Fe_{3-x}GeTe_2$ were grown by the chemical vapor transport technique. Stoichiometric quantities of Fe (STREM Chemicals, Inc., 99.99%), Ge (Acros Organics, 99.999%), and Te (Alfa Aesar, 99.99%) powders along with 5 mg cm^{-3} of iodine transport agent were sealed in quartz ampules. The growth of the single crystals was achieved using a two-zone furnace by holding the source part of the tube at 750 °C and the sink part to 675 °C for 2 weeks, before cooling to room temperature. Silvery metallic platelet single crystals of area 2 × 2 mm^2 were obtained.[56] EDX measurements found the composition of the two chosen samples to be $x = 0.03$ and 0.27. Magnetometry measurements were performed on portions of the bulk crystal using an MPMS3 vibrating sample magnetometer, yielding measured T_C values of 213 and 185 K for the $x = 0.03$ and 0.27 compositions, respectively (Figure S1, Supporting Information).

An all-dry viscoelastic transfer method was used to prepare exfoliated FGT flakes on Si_3N_4 membranes. First, the FGT bulk crystal was mechanically cleaved and exfoliated onto a PDMS stamp. Flakes with a thickness of around 80 nm were selected by inspection of their contrast under an optical microscope, and stamped onto the Si_3N_4 membrane. Skyrmions have previously been observed in FGT flakes with thicknesses between 30 and 400 nm.[42,43] The FGT flakes were then capped by exfoliated hexaboron nitride (hBN) with thickness ≈15 nm, using the same transfer process. The entire fabrication was performed under ambient conditions, which each side of the FGT flakes being exposed to the atmosphere for around 20 min. Thus, we expect around 5 nm of the top and bottom surfaces of each FGT flake to be oxidized.[43] The thicknesses of the final FGT/hBN heterostructures were measured with atomic force microscopy using a Bruker Dimension Icon (Figure S1, Supporting Information). Apart from Figures 1d and 4b, all presented STXM images are of the $x = 0.27$ sample.

Scanning Transmission X-Ray Microscopy: Scanning transmission X-ray microscopy measurements were carried out at the MAXYMUS endstation at the BESSY II electron storage ring operated by the Helmholtz–Zentrum Berlin für Materialien und Energie. The Si_3N_4 chip sample was fixed to the sample holder, and placed into the vacuum chamber of the X-ray microscope. The X-ray beam was tuned to the Fe L_3 edge at a nominal energy of 708 eV, exploiting the resonant absorption effects of X-ray circular dichroism to achieve magnetic contrast.[66] This yields an X-ray absorption proportional to the out-of-plane magnetization, m_z. The transmitted X-ray intensity through the FGT flakes was measured by an avalanche photodiode. The variable out-of-plane magnetic field was achieved by altering the arrangement of four permanent magnets, while the sample temperature was regulated by a liquid He cryostat. The spatial resolution of the technique is estimated to be 25 nm.

Image Processing and Analysis: All presented X-ray microscopy images are the result of subtracting an image of the sample saturated at high applied magnetic field from that of an image acquired under the labeled conditions at the same positive circular X-ray polarisation. This results in the removal of the structural contrast, leaving a view of the magnetic domain states. The domain wall view images presented in Figure 2 were acquired using a Canny edge detection algorithm. The algorithm was applied to the background subtracted image, with the threshold parameters adjusted to achieve an initial representation of the domain wall structure. This was then manually cleaned up, primarily to remove the lines created by detection of the edge of the sample (e.g., shown in Figure S5, Supporting Information).

We extracted the size of all skyrmionium states observed following the ZFC seeding process. Figure S9a,b (Supporting Information) demonstrates the behavior of two example skyrmioniums as a function of increasing field. By acquiring m_z profiles along the largest and shortest axes of each skyrmionium, Gaussian fits of each domain wall were performed to acquire the two elliptical half axes a and b, and thus the corresponding area $A = \pi ab$. For the X-ray microscopy images acquired at each magnetic field, we identified the existing skyrmionium states and similarly approximated the shape of each as an ellipse, such that the area of each individual skyrmionium state could be tracked from the field that they emerged until the field at which they were annihilated (as plotted in Figure S9 (Supporting Information). Finally, the average area of all observed skyrmions as a function of the applied field and the sample temperature was determined (plotted in Figure S9e,f, Supporting Information).

Lorentz Transmission Electron Microscopy: We prepared exfoliated FGT $x = 0.27$ flakes on transmission electron microscopy (TEM)-ready Si_3N_4 membrane windows in the same manner as described above. These specimens were imaged in low-magnification TEM mode with the objective and mini-condenser lenses turned off (Lorentz mode) in a Talos F200X S/TEM under 200 keV acceleration voltage. The samples were cooled to $T = 97$ K $< T_C$ in a Gatan 636 double tilt liquid nitrogen cooling holder. Images were acquired at zero applied field at a range of tilt angles (shown in Figures S2 and S3, Supporting Information), revealing magnetic contrast consistent with Néel-type domain walls. Skyrmionium states were observed after the application of 55 mT using the objective lens.

Micromagnetic Simulations: Micromagnetic simulations following the Landau–Lifshitz–Gilbert (LLG) equation were performed using the MicroMagnum framework with custom extensions for the DMI and thermal fluctuations, utilizing an Euler-type solver with fixed 10 fs time stepping and a spatially and temporally decorrelated thermal field.[67] The simulations were designed to closely model the ZFC procedure performed experimentally, and thus the saturation magnetization was implemented to follow the experimental trend. The simulated area was a square of 1 µm side length, 20 nm thickness and $1000 \times 1000 \times 1$ cells. The ZFC process was performed with a 5 ns duration after an initial 1 ns equilibration period above the micromagnetic T_C (the temperature setting calibrated to where all magnetization becomes fully random).

After the cooling had reached a value of 60% T_C, the temperature was fixed and held at this value (at this point with an $M_s = 45200$ A m^{-1}). Note that thermal fluctuations in micromagnetics utilizing the LLG equation are inherently only an approximate process due to the inability of the LLG to model changes in the magnitude of the magnetic moment and the high-temperature cut-off of spin waves due to a finite cell size. In this case, the method is used to model the introduction of randomness into the magnetic system in a manner that is as close to the experiment as possible. Alternatively, it is possible that random initial states and time-variant magnetic properties could create analogous loop-like features, underlining the universality of the process that does not necessarily depend on the specific mechanism inducing the random magnetization state. An anisotropy field of $H_K = 400$ mT, damping constant $\alpha = 0.5$, exchange stiffness $A = 0.7$ pJ m^{-1} and a DMI of $D = 0.12$ mJ m^{-2} were used for the subsequent field application process. This was performed at a range of fields, with relaxation at each field point. No initial magnetization pattern or manipulation was used, such that the results present a close representation of a zero-field cooling process through T_C. Note that the utilized parameters are not equal to the experimentally measured ones, but correspond to effective values that reproduce the relative size of the skyrmionium loops in the available simulation area. The size of the experimentally observed area would not be feasible to simulate within a reasonable time frame.

Supporting Information

Supporting Information is available from the Wiley Online Library or from the author.

Acknowledgements

Conflict of Interest

The authors declare no conflict of interest.

Data Availability Statement

The data that support the findings of this study are available from the corresponding author upon reasonable request.

Keywords

[1] T. H. R. Skyrme, *Nucl. Phys.* **1962**, *31*, 556.

[2] C. Naya, P. Sutcliffe, *Phys. Rev. Lett.* **2018**, *121*, 23002.

[3] R. A. Battye, M. Haberichter, *Phys. Rev. D* **2013**, *88*, 125016.

[4] N. Nagaosa, Y. Tokura, *Nat. Nanotechnol.* **2013**, *8*, 899.

[5] S. Mühlbauer, B. Binz, F. Jonietz, C. Pfleiderer, A. Rosch, A. Neubauer, R. Georgii, P. Böni, *Science* **2009**, *323*, 915.

[6] X. Z. Yu, Y. Onose, N. Kanazawa, J. H. Park, J. H. Han, Y. Matsui, N. Nagaosa, Y. Tokura, *Nature* **2010**, *465*, 901.

[7] P. J. Ackerman, R. P. Trivedi, B. Senyuk, J. van de Lagemaat, I. I. Smalyukh, *Phys. Rev. E* **2014**, *90*, 012505.

[8] I. I. Smalyukh, Y. Lansac, N. A. Clark, R. P. Trivedi, *Nat. Mater.* **2010**, *9*, 139.

[9] M. Z. Hasan, K. L. Cane, *Rev. Mod. Phys.* **2010**, *82*, 3045.

[10] Y. Tokura, K. Yasuda, A. Tsukazaki, *Nat. Rev. Phys.* **2019**, *1*, 126.

[11] C. N. Weiler, T. W. Neely, D. R. Scherer, A. S. Bradley, M. J. Davis, B. P. Anderson, *Nature* **2008**, *455*, 948.

[12] C. Moreau-Luchaire, C. Moutafis, N. Reyren, J. Sampaio, C. A. F. Vaz, N. Van Horne, K. Bouzehouane, K. Garcia, C. Deranlot, P. Warnicke, P. Wohlhüter, J.-M. George, M. Weigand, J. Raabe, V. Cros, A. Fert, *Nat. Nanotechnol.* **2016**, *11*, 444.

[13] S. Woo, K. Litzius, B. Krüger, M.-Y. Im, L. Caretta, K. Richter, M. Mann, A. Krone, R. M. Reeve, M. Weigand, P. Agrawal, I. Lemesh, M.-A. Mawass, P. Fischer, M. Kläui, G. S. D. Beach, *Nat. Mater.* **2016**, *15*, 501.

[14] C. Back, V. Cros, H. Ebert, K. Everschor-Sitte, A. Fert, M. Garst, T. Ma, S. Mankovsky, T. L. Monchesky, M. Mostovoy, N. Nagaosa, S. S. P. Parkin, C. Pfleiderer, N. Reyren, A. Rosch, Y. Taguchi, Y. Tokura, K. von Bergmann, J. Zang, *J. Phys. D: Appl. Phys.* **2020**, *53*, 363001.

[15] Q. L. He, T. L. Hughes, N. P. Armitage, Y. Tokura, K. L. Wang, *Nat. Mater.* **2022**, *21*, 15.

[16] F. Zheng, F. N. Rybakov, A. B. Borisov, D. Song, S. Wang, Z.-A. Li, H. Du, N. S. Kiselev, J. Caron, A. Kovács, M. Tian, Y. Zhang, S. Blügel, R. E. Dunin-Borkowski, *Nat. Nanotechnol.* **2018**, *13*, 451.

[17] H. Jani, J.-C. Lin, J. Chen, J. Harrison, F. Maccherozzi, J. Schad, S. Prakash, C.-B. Eom, A. Ariando, T. Venkatesan, P. G. Radaelli, *Nature* **2020**, *590*, 74.

[18] F. Zheng, N. S. Kiselev, L. Yang, V. M. Kuchkin, F. N. Rybakov, S. Blügel, R. E. Dunin-Borkowski, *Nat. Phys.* **2022**, *18*, 863.

[19] X. Z. Yu, W. Koshibae, Y. Tokunaga, K. Shibata, Y. Taguchi, N. Nagaosa, Y. Tokura, *Nature* **2018**, *564*, 95.

[20] A. K. Nayak, V. Kumar, T. Ma, P. Werner, E. Pippel, R. Sahoo, F. Damay, U. K. Rößler, C. Felser, S. S. P. Parkin, *Nature* **2017**, *548*, 561.

[21] K. Karube, L. Peng, J. Masell, X. Yu, F. Kagawa, Y. Tokura, Y. Taguchi, *Nat. Mater.* **2021**, *20*, 335.

[22] K. Karube, L. Peng, J. Masell, M. Hemmida, H.-A. K. von Nidda, I. Kézsmárki, X. Yu, Y. Tokura, Y. Taguchi, *Adv. Mater.* **2022**, *43*, 2108770.

[23] J. P. Ackerman, J. van de Lagemaat, I. I. Smalyukh, *Nat. Commun.* **2015**, *6*, 6012.

[24] D. Foster, C. Kind, P. J. Ackerman, J.-S. B. Tai, M. R. Dennis, I. I. Smalyukh, *Nat. Phys.* **2019**, *15*, 655.

[25] M. Finazzi, M. Savoini, A. R. Khorsand, A. Tsukamoto, A. Itoh, L. Duó, A. Kirilyuk, Th. Rasing, M. Ezawa, *Phys. Rev. Lett.* **2013**, *110*, 177205.

[26] S. Zhang, F. Kronast, G. van der Laan, T. Hesjedal, *Nano Lett.* **2018**, *18*, 1057.

[27] A. G. Kolesnikov, M. E. Stebliy, A. S. Samardak, A. B. Ognev, *Sci. Rep.* **2018**, *8*, 16966.

[28] N. Kent, N. Reynolds, D. Raftrey, I. T. G. Campbell, S. Virasawmy, S. Dhuey, R. V. Chopdekar, A. Hierro-Rodriguez, A. Sorrentino, E. Pereiro, S. Ferrer, F. Hellman, P. Sutcliffe, P. Fischer, *Nat. Commun.* **2021**, *12*, 1562.

[29] J. Tang, Y. Wu, W. Wang, L. Kong, B. Lv, W. Wei, J. Zang, M. Tian, H. Du, *Nat. Nanotechnol.* **2021**, *16*, 1086.

[30] F. Zheng, F. N. Rybakov, N. S. Kiselev, D. Song, A. Kovács, H. Du, S. Blügel, R. E. Dunin-Borkowski, *Nat. Commun.* **2021**, *12*, 5316.

[31] F. N. Rybakov, N. S. Kiselev, *Phys. Rev. B* **2019**, *99*, 064437.

[32] V. M. Kuchkin, B. Barton-Singer, F. N. Rybakov, S. Blügel, B. J. Schroers, N. S. Kiselev, *Phys. Rev. B* **2020**, *102*, 144422.

[33] K. S. Burch, D. Mandrus, J.-G. Park, *Nature* **2018**, *563*, 47.

[34] C. Gong, X. Zhang, *Science* **2019**, *363*, eavv4450.

[35] M.-G. Han, J. A. Garlow, Y. Liu, H. Zhang, J. Li, D. DiMarzio, M. W. Knight, C. Petrovic, D. Jariwala, Y. Zhu, *Nano Lett.* **2019**, *19*, 7859.

[36] Y. Wu, B. Francisco, Z. Chen, W. Wang, Y. Zhang, C. Wan, X. Han, H. Chi, Y. Hou, A. Lodesani, G. Yin, K. Liu, Y.-t. Cui, K. L. Wang, J. S. Moodera, *Adv. Mater.* **2022**, *34*, 2110583.

[37] B. Ding, Z. Li, G. Xu, H. Li, Z. Hou, E. Liu, X. Xi, F. Xu, Y. Yao, W. Wang, *Nano Lett.* **2019**, *20*, 868.

[38] Y. Wu, S. Zhang, J. Zhang, W. Wang, Y. Lin Zhu, J. Hu, G. Yin, K. Wong, C. Fang, C. Wan, X. Han, Q. Shao, T. Taniguchi, K. Watanabe, J. Zang, Z. Mao, X. Zhan, K. L. Wang, *Nat. Commun.* **2020**, *11*, 3860.

[39] M. Yang, Q. Li, R. V. Chopdekar, R. Dhall, J. Turner, J. D. Carlström, C. Ophus, C. Klewe, P. Shafer, A. T. N'Diaye, J. W. Choi, G. Chen, Y. Z. Wu, C. Hwang, F. Wang, Z. Q. Qiu, *Sci. Adv.* **2020**, *6*, eabb5157.

[40] T.-E. Park, L. Peng, J. Liang, A. Hallal, F. S. Yasin, X. Zhang, S. J. Kim, K. M. Song, K. Kim, M. Weigand, G. Schütz, S. Finizio, J. Raabe, K. Garcia, J. Xia, Y. Zhou, M. Ezawa, X. Liu, J. Chang, H. C. Koo, Y. D. Kim, M. Chshiev, A. Fert, H. Yang, X. Yu, S. Woo, *Phys. Rev. B* **2021**, *103*, 104410.

[41] L. Peng, F. S. Yasin, T.-E. Park, S. J. Kim, X. Zhang, T. Nagai, K. Kimoto, S. Woo, X. Yu, *Adv. Funct. Mater.* **2021**, *31*, 2103583.

[42] A. Chakraborty, A. K. Srivastava, A. K. Sharma, A. K. Gopi, K. Mohseni, A. Ernst, H. Deniz, B. K. Hazra, S. Das, P. Sessi, I. Kostanovskiy, T. Ma, H. L. Meyerheim, S. S. P. Parkin, *Adv. Mater.* **2022**, *34*, 2108637.

[43] M. T. Birch, L. Powalla, S. Wintz, O. Hovorka, K. Litzius, J. C. Loudon, L. A. Turnbull, V. Nehruji, K. Son, C. Bubeck, T. G. Rauch, M. Weigand, E. Goering, M. Burghard, G. Schütz, *Nat. Commun.* **2022**, *13*, 3035.

[44] C. Xu, X. Li, P. Chen, Y. Zhang, H. Xiang, L. Bellaiche, *Adv. Mater.* **2022**, *34*, 2107779.

[45] H. Li, S. Ruan, Y.-J. Zeng, *Adv. Mater* **2019**, *31*, 1900065.

[46] S.-J. Liang, B. Cheng, X. Cui, F. Miao, *Adv. Mater* **2020**, *32*, 1903800.

[47] I. Žutić, A. Matos-Abiague, B. Scharf, H. Dery, K. Belashchenko, *Mater. Today* **2019**, *22*, 85.

[48] B. Huang, M. A. McGuire, A. F. May, D. Xiao, P. Jarillo-Herrero, X. Xu, *Nat. Mater.* **2020**, *19*, 1276.

[49] M. Bora, P. Deb, *J. Phys.: Mater.* **2021**, *4*, 034014.

[50] Z. Wang, Z. Wang, D. Sapkota, T. Taniguchi, K. Watanabe, D. Mandrus, A. F. Morpurgo, *Nano Lett.* **2018**, *18*, 4303.

2208930 (8 of 9)

[51] X. Li, J.-T. Lü, J. Zhang, L. You, Y. Su, E. Y. Tsymbal, *Nano Lett.* **2019**, *19*, 5133.

[52] S. Albarakati, C. Tan, Z.-J. Chen, J. G. Partridge, G. Zheng, L. Farrar, E. L. H. Mayes, M. R. Field, C. Lee, Y. Wang, Y. Xiong, M. Tian, F. Xiang, A. R. Hamilton, O. A. Tretiakov, D. Culcer, Y.-J. Zhao, L. Wang, *Sci. Adv.* **2019**, *5*, eaaw0409.

[53] B. Zhao, R. Ngaloy, A. Md. Hoque, B. Karpiak, D. Khokhriakov, S. P. Dash, *arXiv Preprint*, **2022**.

[54] Z. Fei, B. Huang, P. Malinowski, W. Wang, T. Song, J. Sanchez, W. Yao, D. Xiao, X. Zhu, A. F. May, W. Wu, D. H. Cobden, J.-H. Chu, X. Xu, *Nat. Mater.* **2018**, *17*, 778.

[55] H.-J. Deiseroth, K. Aleksandrov, C. Reiner, L. Kienle, R. K. Kremer, *Eur. J. Inorg. Chem.* **2006**, 1561.

[56] D. A. Mayoh, G. D. A. Wood, S. J. R. Holt, G. Beckett, E. J. L. Dekker, M. R. Lees, G. Balakrishnan, *Cryst. Growth Des.* **2021**, *21*, 6786.

[57] A. F. May, S. Calder, C. Cantoni, H. Cao, M. A. McGuire, *Phys. Rev. B* **2016**, *93*, 014411.

[58] S. Y. Park, D. S. Kim, Y. Liu, J. Hwang, Y. Kim, W. Kim, J.-Y. Kim, C. Petrovic, C. Hwang, S.-K. Mo, H.-j. Kim, B.-C. Min, H. C. Koo, J. Chang, C. Jang, J. W. Choi, H. Ryu, *Nano Lett.* **2020**, *20*, 95.

[59] B. Seng, D. Schönke, J. Yeste, R. M. Reeve, N. Kerber, D. Lacour, J.-L. Bello, N. Bergeard, F. Kammerbauer, M. Bhukta, T. Ferté, C. Boeglin, F. Radu, R. Abrudan, T. Kachel, S. Mangin, M. Hehn, M. Kläui, *Adv. Func. Mater.* **2021**, *21*, 2102307.

[60] F. Zheng, H. Li, S. Wang, D. Song, C. Jin, W. Wei, A. Kovács, J. Zang, M. Tian, Y. Zhang, H. Du, R. E. Dunin-Borkowski, *Phys. Rev. Lett.* **2017**, *119*, 197205.

[61] S. Finizio, S. Wintz, D. Bracher, E. Kirk, A. S. Semisalova, J. Förster, K. Zeissler, T. Weßels, M. Weigand, K. Lenz, A. Kleibert, J. Raabe, *Phys. Rev. B* **2018**, *98*, 104415.

[62] N. Kent, R. Streubel, C.-H. Lambert, A. Ceballos, S.-G. Je, S. Dhuey, M.-Y. Im, F. Büttner, F. Hellman, S. Salahuddin, P. Fischer, *Appl. Phys. Lett.* **2019**, *115*, 112404.

[63] C. Kind, D. Foster, *Phys. Rev. B* **2021**, *103*, L100413.

[64] A. O. Leonov, C. Pappas, *Phys. Rev. B* **2019**, *99*, 144410.

[65] K. Litzius, J. Leliaert, P. Bassirian, D. Rodrigues, S. Kromin, I. Lemesh, J. Zazvorka, K.-J. Lee, J. Mulkers, N. Kerber, D. Heinze, N. Keil, R. M. Reeve, M. Weigand, B. Van Waeyenberge, G. Schütz, K. Everschor-Sitte, G. S. D. Beach, M. Kläui, *Nat. Electron.* **2020**, *3*, 30.

[66] G. van der Laan, A. I. Figueroa, *Coord. Chem. Rev.* **2014**, *277*, 95.

[67] J. Leliaert, J. Mulkers, J. De Clercq, A. Coene, M. Dvornik, B. Van Waeyenberge, *AIP Adv.* **2017**, *7*, 125010.

2208930 (9 of 9)